JOURNAL OF MATERIALS SCIENCE 13 (1978) 1991–2002

Splat cooling of iron-molybdenum-carbon alloys

I. R. SARE*, R. W. K. HONEYCOMBE
Department of Metallurgy and Materials Science, University of Cambridge, Cambridge, UK

Two molybdenum alloy steels, which normally undergo the austenite → martensite phase transformation during solid state quenching, have been rapidly cooled from the melt in a controlled atmosphere "gun" splat cooling device. The matrix phases produced were δ-ferrite, martensite, and austenite; the carbide Mo_2C was also present in the as-quenched condition in the higher alloy composition studied. The amount of austenite retained to room temperature was found to be inversely related to the cooling rate. The morphology of the martensite in the splat-cooled alloys exhibited a marked change compared with its characteristic appearance in the conventionally solid-state quenched material. This was attributed to the dual effect of increased cooling rate on carbon segregation in the parent austenite and of decreased section thickness in which the martensite forms. The degree of solute segregation observed in the microstructures of the matrix phases was shown to depend on the extent of the equilibrium liquidus–solidus temperature range. The precipitation of Mo_2C during ageing in the range 600 to 700° C paralleled the behaviour of conventionally quenched and tempered alloys, although local inhomogeneities did produce precipitation phenomena not encountered in solid-state quenched material.

1. Introduction

When high alloy steels such as tool steels are solution-treated and quenched, substantial proportions of the alloying element additions are wasted, owing to the insolubility of some alloy carbides at the austenitizing temperature. As a result, the microstructure after quenching is very inhomogeneous, and the full secondary hardening potential of the alloy is unattainable. Greater alloying element solubility can be achieved by rapid quenching from the liquid state (splat cooling), which also avoids complete transformation to martensite in many cases. The present investigation has used this technique in a study of precipitation in some Fe–Mo–C alloys, the behaviour of which during conventional heat treatments is well known [1, 2].

One of the few studies made of splat-cooled ferrous systems was a detailed examination of Fe–C alloys embracing the composition range 0 to 5 wt% carbon [3]. In compositions up to approximately 2 wt% carbon, the maximum equilibrium solubility of carbon in austenite [4], the only phases present after splat cooling were martensite and austenite, the amount of austenite increasing with carbon content. At higher carbon levels up to about 3 wt%, and in the presence of silicon, the predominant phase was austenite, the supersaturation of which reached a maximum of 2.37 wt% carbon. At still higher carbon levels a new hcp metastable phase was predominant. In a subsequent study [5] of Fe–Ni–B alloys, a marked increase of the order of 1000 times in dissolved boron was found in both the austenite and martensite phases compared with the equilibrium solubility of boron in α- and γ-iron [6]. Boron additions up to 2 wt% in Fe–13 wt% Ni and Fe–24 wt% Ni alloys were also found to cause an increase in the amount of retained austenite, from 0 to 59% and 92% respectively. This effect was attributed to depression of the M_s temperature well below that caused by nickel alone,

*Now with CSIRO Division of Materials Science, Adelaide, Australia 5011.

similar to the effect of carbon and nitrogen.

The only reported investigation of ternary low-carbon Fe–C–X alloys, where X is a substitutional carbide-forming alloying element, was made using plasma arc melting and piston-and-anvil type cooling [7]. The cooling rates reached a maximum of only $10^4\,K\,sec^{-1}$, however, at least two orders of magnitude less than those normally encountered in splat cooling work. Optical microscopy of a rapidly cooled ($10^3\,K\,sec^{-1}$) Fe–3.18 wt % Mo–0.2 wt % C alloy revealed only martensite, although extraction replicas observed by transmission electron microscopy showed fine ϵ-carbide particles lying principally along the martensite needles, indicating some tempering of the structure during the quench. Similarly in an Fe–1.32 wt % Ti–0.33 wt % C alloy cooling rates as high as $10^4\,K\,sec^{-1}$ were insufficient to suppress carbide precipitation, although the hardness of the as-quenched alloy did increase with cooling rate, reflecting the finer carbide distribution produced by higher cooling rates. The subsequent precipitation of alloy carbides during ageing of both alloys was confirmed, and secondary hardening was observed to take place.

Two alloys were chosen for study in the present investigation. The first has the nominal composition Fe–4 wt % Mo–0.2 wt % C, and was selected because its behaviour under conventional solid-state quenching and tempering conditions has been well documented [1, 2]. The second alloy, Fe–10 wt % Mo–0.5 wt % C, maintains the same stoichiometric ratio of Mo:C as the first, but always contains residual carbides after high temperature solid-state solution treatment (Fig. 1).

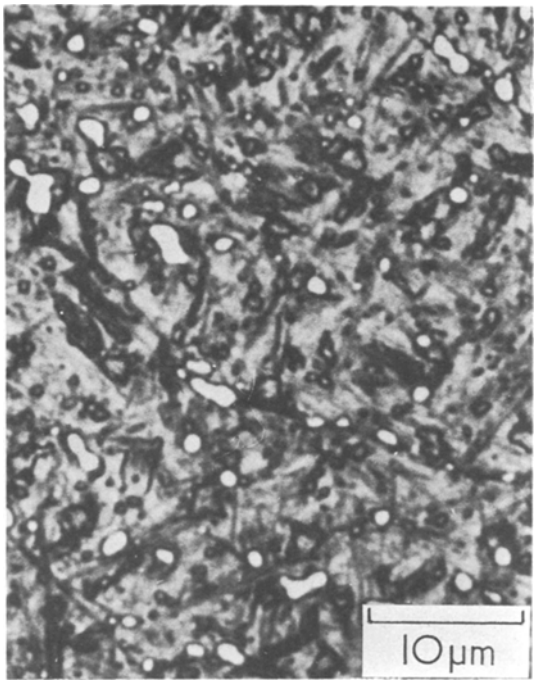

Figure 1 Insoluble carbides in Fe–10% Mo–0.5% C, solution treated for 1 h at 1200° C and water-quenched. Etched in 3% nital. Optical micrograph.

2. Experimental procedure

The two Fe–Mo–C alloys were prepared by melting the high purity constituent elements together in an argon arc furnace. Each ingot was remelted three times prior to removal from the furnace, cut into several pieces, and remelted in the furnace to ensure macroscopic homogeneity. The ingots were then sealed in silica capsules under a partial pressure of argon and homogenized for 50 h at 1200° C. The compositions of the alloys are shown in Table I. The ingots were cold-swaged to 3 mm rods, and the surfaces cleaned by filing to remove any oxide. Small pieces weighing about 0.25 g were cut from the rods for use in the controlled atmosphere "gun" splat cooling apparatus which has been described in detail elsewhere [8].

X-ray analysis of splat-cooled material was carried out by Debye–Scherrer powder photography with iron-filtered cobalt Kα radiation. Lattice parameters were obtained from a weighted least-squares extrapolation against the Nelson–Riley–Taylor–Sinclair function to $\theta = 90°$.

Splat-cooled flakes for scanning electron microscopy were examined in both the "as-splatted" condition, and after electropolishing in 5% perchloric acid in 2-butoxyethanol and etching in 3% nital. Similarly, some flakes for transmission electron microscopy were examined without any prior thinning, and others were either ion-beam thinned or electropolished. All transmission electron microscopy was carried out in a JEOL

TABLE I Alloy Compositions

Designation	Composition (wt %)	
	C	Mo
Fe–4% Mo–0.2% C	0.19	4.20
Fe–10% Mo–0.5% C	0.48	10.40

JEM 200A instrument at an operating voltage of 200 kV.

Heat treatments were performed in sealed silica capsules under a partial pressure of argon. All heat treatments, including the solution treatment stage in the production of quenched filings, were terminated by quenching the specimen in its capsule in water. Differential thermal analysis (DTA) was carried out in a Dupont 900 Thermal Analyser, with the furnace operating under a flow of argon during the heating process. All runs were made at a heating rate of 0.33 K sec^{-1} (20 K min^{-1}), and once the desired temperature had been reached the sample was removed quickly and cooled to room temperature for subsequent X-ray powder analysis.

3. Results

3.1. X-ray diffraction analysis

Face-centred cubic (f c c) austenite and a body-centred cubic (b c c) product were the only phases detected by X-ray diffraction in both alloys in the as-splatted condition. The proportion of austenite varied from run to run with each alloy, but fell within the approximate limits 0 to 5% for Fe–4% Mo–0.2% C and 0 to 10% for Fe–10% Mo–0.5% C. The average lattice parameters of the b c c product are presented in Table II. So few austenite lines appeared on the diffraction patterns of the two Fe–Mo–C alloys that no reliable measurement of its lattice parameter could be made. For comparison Table II also lists the lattice parameter of the martensite present in filings of the respective alloys, prepared by solution treatment for 1 h at 1200° C followed by water quenching.

The lattice parameter determined for the b c c product in the splat-cooled Fe–4% Mo–0.2% C alloys is no higher than that in the water-quenched filings, within the errors of the measurements, since even solid-state solution treatment is able to take all the carbide into solution. In the Fe–10% Mo–0.5% C alloy splat cooling does give a significant increase in the b c c product lattice parameter over that of the water-quenched filings.

Tetragonality was not detected either in the martensite of the quenched filings or in the b c c product of the splat-cooled alloys. This is not unexpected, however, since the broadness of diffraction lines and merging of doublets obscure the tetragonality of martensites containing less than about 0.6% C [9]. In splat-cooled samples, broadening arising from small particle sizes [10] and lattice strain [11] would enhance the broadening due to martensite transformation, and so the absence of tetragonality in X-ray diffraction patterns of these splat-cooled alloys is not surprising.

TABLE II Lattice parameters of the b c c product in splat-cooled material and water-quenched filings

Alloy	Treatment	Lattice parameter (Å)
Fe–4% Mo–0.2% C	splat cooled	2.875 ± 0.004
	filings	2.874 ± 0.001
Fe–10% Mo–0.5% C	splat cooled	2.890 ± 0.003
	filings	2.885 ± 0.001

The variation in the amount of austenite retained to room temperature from run to run was found to be a result of cooling rate fluctuations. This was verified by some trials with the Fe–4% Mo–0.2% C alloy in which the copper substrate was deliberately allowed to oxidize in air for several days before insertion in the specimen chamber. X-ray analysis of the splat-cooled material produced under these conditions showed a marked increase in the proportion of austenite present. Therefore, austenite retention in these alloys is favoured by relatively slow cooling rates, induced by the poorer thermal contact achieved when the copper substrate has a thin surface layer of oxide.

3.2. Scanning electron microscopy of the as splat-cooled alloys

The microstructural features of splat-cooled alloys are generally too small to be resolved in the optical microscope and one needs to resort to scanning electron microscopy to obtain an overall view of the microstructure. Fig. 2a is a scanning electron micrograph of a flake of the Fe–4% Mo–0.2% C alloy, electropolished and etched in 3% nital. The solidification cells or dendrites are just visible within the equiaxed grains, whose size ranges over an order magnitude from about 0.5 to 5 μm. Similarly-prepared flakes of the Fe–10% Mo–0.5% C alloy showed thin films of second phase particles decorating the dendrite boundaries (Fig. 2b).

3.3. Transmission electron microscopy of the as splat-cooled alloys

3.3.1. Fe–4% Mo–0.2% C

Detailed examination by transmission electron microscopy reveals the most significant features of

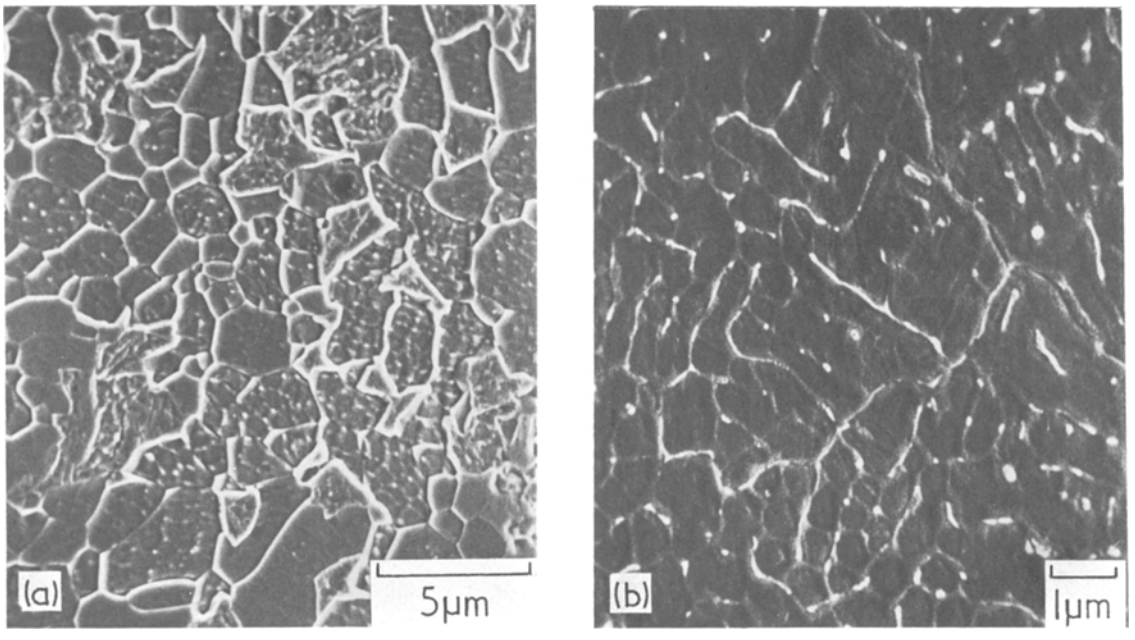

Figure 2 Scanning electron micrographs of splat-cooled flakes, electropolished and etched in 3% nital: (a) Fe–4% Mo–0.2% C, (b) Fe–10% Mo–0.5% C.

the microstructures. In unthinned regions of the Fe–4% Mo–0.2% C alloy ferritic (b c c) areas invariably consisted of grains elongated in the plane of the foil, exhibiting no sign of any cellular or dendritic structure (Fig. 3a) and possessing a low dislocation density. Areas exhibiting this type of grain morphology have been shown [12] to be indicative of heat extraction during solidification taking place parallel to the plane of the foil. For comparison Fig. 3b shows the martensitic structure found in the same alloy after water quenching from 1200° C. It is apparent that the

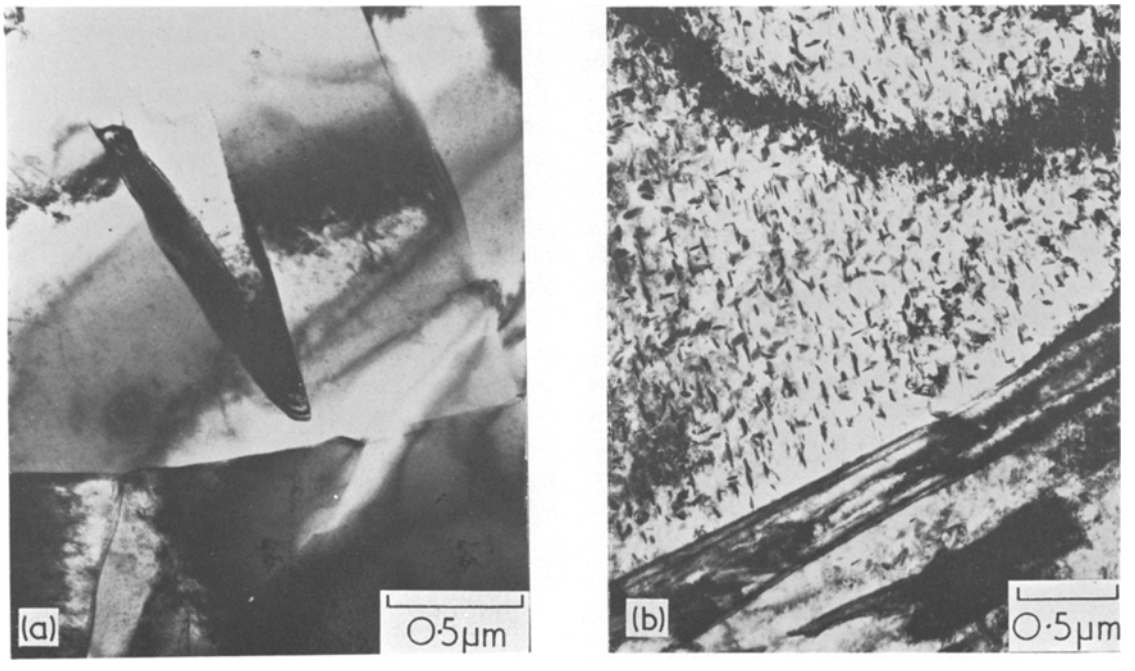

Figure 3 Transmission electron micrographs of Fe–4% Mo–0.2% C; (a) elongated ferrite grains in an unthinned foil of the splat-cooled alloy, (b) autotempered martensite in an electropolished thin foil of the water-quenched alloy.

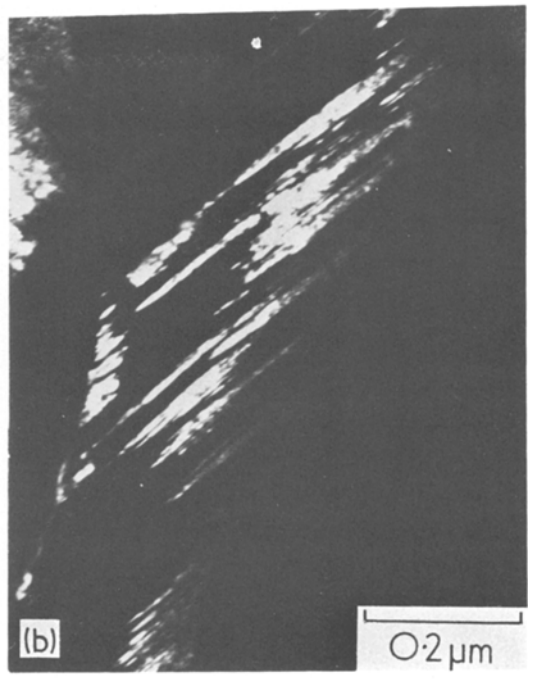

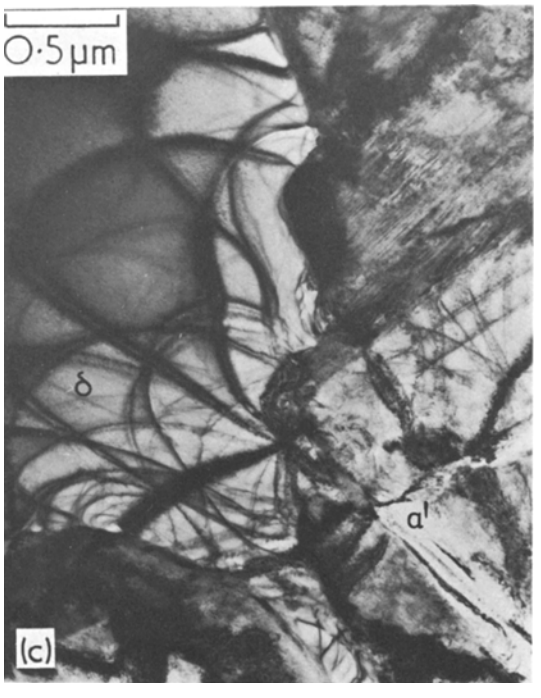

Figure 4 Transmission electron micrographs of electropolished foils of splat-cooled Fe–4% Mo–0.2% C; (a) twinned martensite – bright field image, (b) same area as (a) – dark field, imaged with a martensite twin spot, (c) twinned martensite (α') and distorted ferrite (δ).

splat-cooled ferrite is not martensitic since it does not contain the laths typical of low-carbon martensites, nor a sufficiently high dislocation density.

Martensite was observed, however, in foils of this alloy thinned by electropolishing. Figs. 4a and b are a bright field–dark field pair showing {1 1 2} twins in a martensite matrix. Fig. 4c is a micrograph which shows adjacent areas of ferrite and finely twinned martensite. The ledges on the interface between the martensite and ferrite suggest that at some earlier stage one of the phases was growing into the other. The most likely explanation is that the material originally solidified as high temperature δ-ferrite*, and that as cooling proceeded austenite nucleated and started to grow into the δ-ferrite. However, the cooling rate was so high that this reaction could not go to completion, and the austenite which had formed subsequently transformed to martensite below its M_s temperature.

Splats of material from those runs with the Fe–4% Mo–0.2% C alloy which yielded a considerable proportion of austenite were examined in order to characterize the morphology of the austenite. Unthinned foils again revealed grains elongated in the plane of the foil (Fig. 5). The

*The term "δ-ferrite" is used throughout this paper to denote ferrite formed at high temperatures, whether the equilibrium diagram for the alloy in question contains two distinct ferrite phase fields (α and δ) or only one ferrite phase field which extends right up to the solidus.

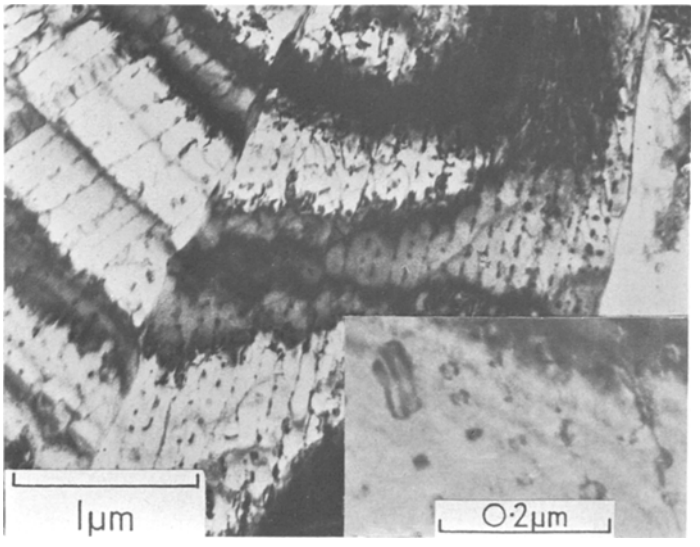

Figure 5 Austenite in an unthinned foil of splat-cooled Fe–4% Mo–0.2% C. Transmission electron micrograph of elongated grains showing linear arrays of defects. The insert is a higher magnification micrograph showing rows of dislocation loops which constitute the linear arrays.

grains contain linear arrays of defects lying in $\langle 1\,0\,0\rangle_\gamma$ directions, and the higher magnification micrograph shown as an insert in Fig. 5 indicates that the defects may be dislocation loops. No detailed examination was made of the nature of the loops, but in view of the similarity between the rows of defects in the austenite observed here and those observed in a splat-cooled Fe–20% Cr–25% Ni alloy [13], it is a reasonable inference that the loops are also of the vacancy coalescence type.

3.3.2. Fe–10% Mo–0.5% C

Several distinct matrix morphologies of the b c c product were observed in the Fe–10% Mo–0.5% C alloy, but no austenite was ever recognized. Unthinned foils of ferrite showed a fine dendritic structure (Fig. 6a), in which dendrite growth had apparently occurred in the plane of the foil. A few unthinned areas also revealed a finely twinned martensitic structure (Fig. 6b). The existence of second phase particles at the interdendritic ferrite boundaries observed by scanning electron microscopy (Fig. 2b) was confirmed in ion-beam thinned material (Fig. 6c), and at the same time the presence of fine precipitate needles within the dendrites was detected. In this micrograph there are obvious precipitate-free zones between this fine matrix precipitate and the large boundary particles. Electron diffraction and dark-field microscopy showed that the coarse interdendritic particles and fine matrix precipitate are Mo_2C, obeying the usual Pitsch and Schrader [14] orientation relationship with the ferrite, namely:

$$(2\,\bar{1}.0)\ Mo_2C \parallel (1\,0\,0)\ \text{ferrite}$$

$$(0\,1.0)\ Mo_2C \parallel (0\,1\,\bar{1})\ \text{ferrite}$$

$$(0\,0.1)\ Mo_2C \parallel (0\,1\,1)\ \text{ferrite}.$$

The fact that the dendrite arm spacing in Fig. 6c (approximately 0.5 μm) is larger than the average secondary dendrite arm spacing in Fig. 6a (0.25 μm) indicates that the latter is from a faster cooled region. This difference in cooling rate between these two areas reflects the difference in initial thickness, since Fig. 6a is a micrograph from an unthinned area whilst Fig. 6c is from an ion-beam thinned, and hence initially thicker, foil. Furthermore, the presence of precipitate particles at the interdendritic boundaries in Fig. 6c confirms that this area cooled more slowly than that in Fig. 6a, where no interdendritic precipitate was detected.

The presence of Mo_2C needles within the dendrites of Fig. 6c is not a result of the solute segregation during solidification which led to the precipitation at the interdendritic boundaries, but indicates that cooling was sufficiently slow after solidification had occurred to permit the diffusion of molybdenum and carbon atoms. This is analogous to the autotempering of low-carbon martensites (Fig. 3b), in which Fe_3C precipitation takes place during the quench below the M_s temperature (that is, below about 400° C). In the splat-cooled Fe–10% Mo–0.5% C alloy the precipitation of Mo_2C must take place at much higher temperatures than this during the quench, since diffusion of both molybdenum and carbon is necessary, whereas in the auto-tempering of

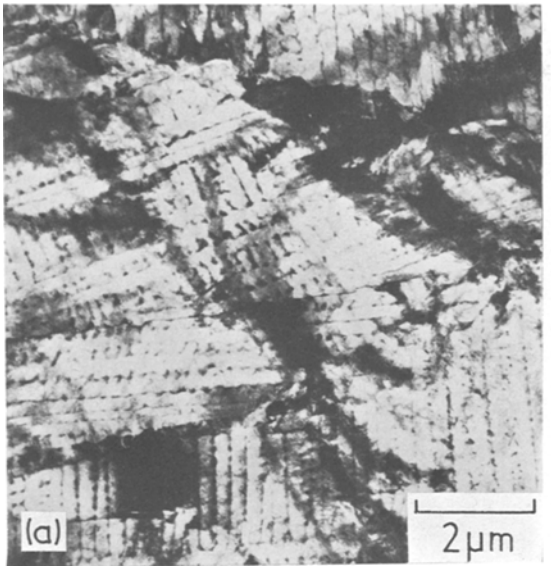

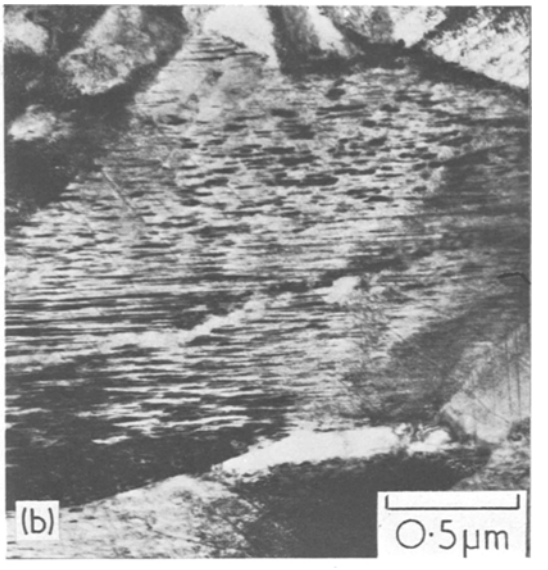

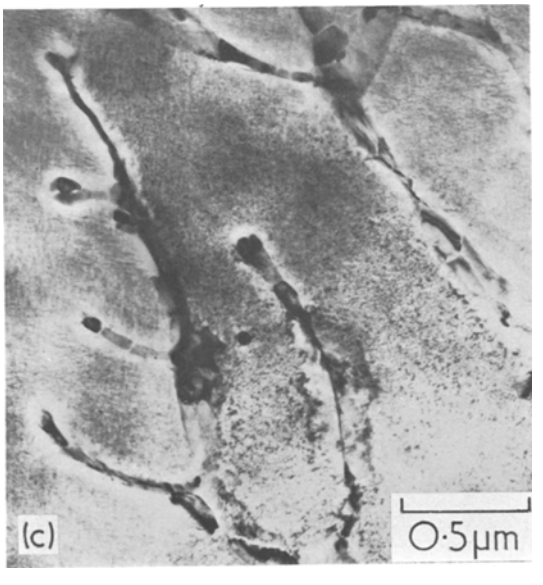

Figure 6 Transmission electron micrographs of splat-cooled Fe–10% Mo–0.5% C; (a) primary and secondary dendrites in an unthinned foil, (b) finely-twinned martensite in an unthinned foil, (c) ion-beam thinned foil showing Mo_2C precipitation at the interdendritic boundaries and within the dendrites.

martensite only carbon atom diffusion is required. However, since the solid solution in the case of the splat-cooled alloy is supersaturated even at its freezing temperature, precipitation will commence as soon as the solid is formed.

3.4. Ageing of the splat-cooled alloys

3.4.1. Differential thermal analysis

In the Fe–4% Mo–0.2% C alloy, samples from splat cooling runs containing the b c c product alone, and the b c c product plus austenite, were heated in the DTA apparatus to 500° C. Material containing only the b c c product gave no peaks in the ΔT versus temperature plot, but material which contained both austenite and the b c c product gave a small, broad, exothermic peak in the range 220 to 400° C. X-ray diffraction patterns taken from this material after it had cooled to room temperature showed that the f c c austenite had disappeared, and the only phase detected was the b c c product.

Differential thermal analysis of samples of the Fe–10% Mo–0.5% C alloy containing austenite showed no decomposition peak upon continuous heating to 600° C, the upper temperature limit of the furnace. However, isothermal ageing in the DTA apparatus for 1 h at various temperatures, followed by X-ray analysis, revealed that all retained austenite disappeared between 1 h at 550° C and 1 h at 600° C. That is, after 1 h at 550° C no change in the amount of austenite present was detected, but after 1 h at 600° C the austenite had completely disappeared.

3.4.2. Metallography

Fig. 7 illustrates the microstructure of splat-cooled Fe–4% Mo–0.2% C after ageing for 1 h at 600° C, in which fine needles of Mo_2C have precipitated in the ferrite matrix. The needles precipitated according to the Pitsch and Schrader [14] orientation relationship, and electron diffraction patterns con-

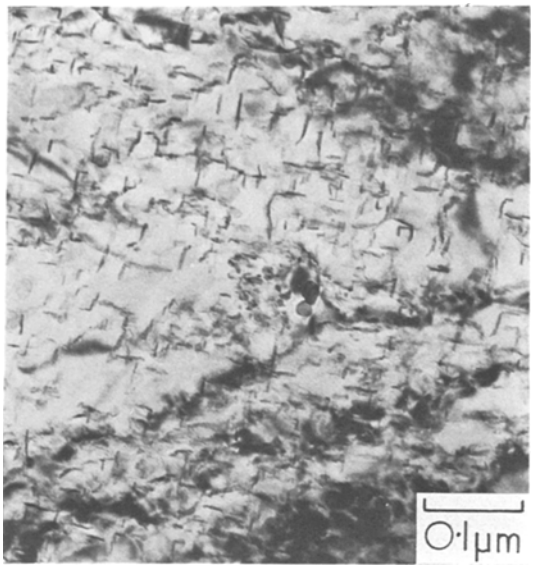

Figure 7 Mo_2C needles in splat-cooled Fe–4% Mo–0.2%C, aged 1 h at 600° C. Electropolished foil. Transmission electron micrograph.

Figure 8 Electropolished foil of splat-cooled Fe–10% Mo–0.5% C aged 20 h at 600° C, showing the three variants of Mo_2C needles within the dendrites of the solidification structure. Transmission electron micrograph.

tained heavy streaking in ⟨1 0 0⟩ ferrite directions, as observed previously [1] during the early stages Mo_2C precipitation. Over-ageing in the two splat-cooled Fe–Mo–C alloys occurred by the growth of the Mo_2C needles, with re-solution of the smaller needles in favour of the larger ones. Fig. 8 shows the splat-cooled Fe–10% Mo–0.5% C alloy aged for 20 h at 600° C, in which the three orthogonal variants of Mo_2C needle precipitation are clearly visible within the dendrites of the solidification structure. The interdendritic precipitate species is still Mo_2C.

In some areas of this alloy precipitation of large M_6C particles was observed adjacent to small, apparently recrystallized, ferrite grains. In Fig. 9 the M_6C carbides are the large, black, irregularly-shaped particles associated with some of the recrystallized ferrite grains. Such areas were observed only in small localized regions, and the periphery of Fig. 9 shows the Mo_2C needle precipitate typical of most of the microstructure.

A further microstructural feature observed in a few small areas of the aged Fe–10% Mo–0.5% C alloy was the discontinuous precipitation reaction product shown in Fig. 10. The coarse lamellae of carbide were identified as Mo_2C. Adjacent to the grains containing this particular morphology of Mo_2C the normal continuous precipitation of Mo_2C needles was still apparent, and so both

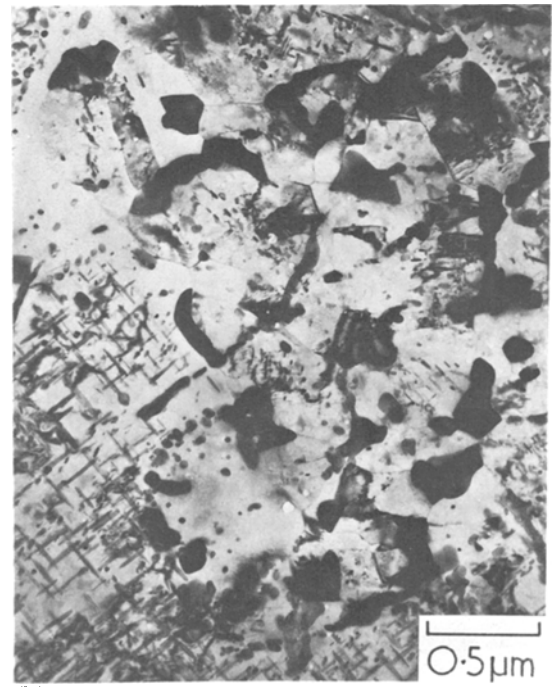

Figure 9 Precipitation of M_6C carbides (black globular particles) and recrystallization of small ferrite grains in splat-cooled Fe–10% Mo–0.5% C aged 20 h at 600° C. Electropolished foil. Transmission electron micrograph.

forms of the carbide co-existed within the one small area.

4. Discussion

4.1. The nature of the b c c product

Two sets of crystalline reflections were detected by X-ray diffraction analysis of the splat-cooled alloys. One could be indexed as f c c austenite, and the other as a b c c product. It has already been shown that the absence of tetragonality in the latter cannot be taken as evidence that it is not martensitic, because tetragonality was not observed in the martensite lines of the water-quenched filings either. The metallographic evidence, however, suggests that the b c c product consists of two phases – δ-ferrite and martensite. In the Fe–4% Mo–0.2% C alloy it was shown that martensite is present in thin foils (Fig. 4). The morphology of the b c c product in Fig. 3a, however, does not resemble any of the usual microstructures attributed to martensite, and therefore it must be δ-ferrite, cooled too rapidly to nucleate austenite. The fact that the elongated grains were observed in unthinned areas means that they are in the thinnest, and hence fastest-cooled parts of the foil. Speich [15] has observed that rapid quenching from the solution treatment temperature into water of some binary Fe–Nb alloys results in the retention of the δ-phase without transformation to austenite, and hence to martensite. Clearly, therefore, austenite is more likely to be found in the thicker regions of the splats, and consequently these will also be the places where martensite will occur.

Scanning electron microscopy of the Fe–10% Mo–0.5% C alloy revealed only regions of a dendritic or cellular solidification morphology (Fig. 2b), which were found by transmission electron microscopy to be ferritic (Figs. 6a and c). Small regions of martensite were observed however (Fig. 6b), confirming that the b c c product detected by X-ray diffraction in this alloy is a mixture of δ-ferrite and martensite, as in the Fe–4% Mo–0.2% C alloy.

4.2. The occurrence of austenite

The fact that in the Fe–4% Mo–0.2% C alloy more austenite is retained to room temperature when the cooling rate is lower than normal depends on two factors: the formation of austenite from the liquid plus δ-ferrite and the stabilization of the austenite once it has formed. It has already been shown that at very high rates of cooling there may be insufficient time for transformation of δ to γ to occur before the temperature falls to a level where atomic diffusion is prohibitively slow. On the other hand if the cooling rate is lower δ-ferrite can transform to austenite, the extent of transformation depending on how low the cooling rate actually is.

In the conventional heat treatment of alloy steels, the amount of retained austenite increases with decreasing cooling rate provided the quenching rate is sufficient to avoid the formation of ferrite and pearlite [16, 17]. This stabilization of austenite has been attributed to the segregation of carbon to lattice defects in the austenite, thus increasing its resistance to shear transformation [17, 18]. It is possible that such an explanation could apply to the higher cooling rates involved in splat quenching, as there is certainly evidence for carbon diffusion during the quench. However in other alloys, e.g. Fe–Ni [19], austenite retention is enhanced at relatively high cooling rates, so the matter needs further detailed study.

4.3. Solidification morphologies of δ-ferrite

The micrographs of splat-cooled foils for both alloys show different morphologies of the δ-ferrite. In the Fe–4% Mo–0.2% C alloy the ferritic regions in thin foils are grains showing no evidence of solute segregation, while in the Fe–10% Mo–0.5% C alloy the ferritic regions exhibit a cellular or dendritic solidification structure, with the segregation of solute to, and formation of carbide at the interdendritic boundaries.

The segregation effects associated with cellular and dendritic growth require that solidification takes place between the liquidus and solidus temperatures, for a given alloy composition. In this way solute-lean solid can crystallize (for a distribution coefficient less than unity) and produce solute enrichment of the surrounding liquid, so that when solidification is completed there is segregated solute at the cell walls and interdendritic boundaries. If the liquid is undercooled below the solidus, however, solute segregation is not possible and the entire alloy will solidify with the mean composition of the liquid [20, 21], provided that recalescence does not reach the solidus temperature [22]. Large undercoolings would be expected to occur at the very high rates of solidification found in splat cooling.

Thus, depending on the range between the liquidus and solidus temperatures, solidification may occur with or without concomitant segregation.

Vertical sections of the ternary equilibrium diagrams of Fe–4%Mo–0.2%C and Fe–10% Mo–0.5%C [23] indicate that the former alloy has a freezing range of approximately 50 K whilst the range in the latter is about 150 K. Experimental determinations [22, 24] of the amount of undercooling taking place during splat cooling give values in excess of 100 K, and so the former will solidify as a homogeneous solid solution below its solidus temperature, whilst the latter is more likely to crystallize between its liquidus and solidus temperatures and thus exhibit solute segregation, as is observed to be the case.

4.4. The morphology of the martensite

Both alloys, after splat cooling, contained areas of twinned plate martensite which is quite different from the dislocated lath martensite observed in the solid-state quenched material. This change in morphology with increasing quench rate has been observed several times previously in solid-state quenched martensites [25, 26] and has been attributed to the increase of M_s temperature which results. Measurements [17, 18, 25, 26] of the M_s temperature for a number of Fe–C and Fe–C–X alloys over a quench rate range from 5×10^3 to 3×10^4 K sec^{-1} have shown that the M_s increases by up to 110 K in a sigmoidal fashion. In this range, the morphology of Fe–Ni–C martensites changes from a dislocated lath structure in slow-quenched samples to a twinned plate structure in the fast quenched samples. As mentioned earlier, carbon segregation is less at higher quench rates, so the austenite is not so effectively stabilized, and thus has a higher M_s temperature

The present work confirms the trends previously observed in the Fe–Ni–C alloys in so far as the morphological changes are concerned. However caution must be observed in comparing the results on splat-quenched material with those on conventional specimens, because Pitsch [27, 28] has shown that the martensite formed in thin films of Fe–C and Fe–N alloys transforms by a different mechanism from the bulk material, and has a different microstructure. Furthermore, the M_s temperature of the martensite which forms in Fe–C and Fe–Ni alloys during electrochemical thinning has been found to be considerably higher than that of the bulk material [29, 30].

4.5. The microstructures obtained on ageing

The precipitation of Mo_2C needles in both alloys parallels the behaviour of conventionally quenched and tempered material [1], although the matrix is δ-ferrite and not tempered martensite. However, some important differences were evident in the Fe–10%Mo–0.5%C alloy. The appearance of recrystallization in certain areas (Fig. 9) after only 20 h at 600° C must be associated with some local inhomogeneity. The existence of strain in splat-cooled material has been shown by recent work on X-ray line broadening [11], and because of the variation of cooling conditions within any given splat, inhomogeneous distribution of this strain is quite possible. The small region of recrystallization in Fig. 9 may be a result of such an inhomogeneous strain distribution, since recrystallization will begin at a lower temperature or at shorter times in areas where the local strain is higher.

Alternatively, the inhomogeneity may have been in the original solute distribution. If, as a result of solute segregation, the Mo/C atomic ratio were higher in the central area of Fig. 9 than around the periphery, the formation of globular M_6C particles would have been preferred over the precipitation of Mo_2C needles [31]. On the assumption that the strain in this case is homogeneously distributed, then the nature of the precipitate dispersion would be the factor governing whether recrystallization would occur [32]. If the particles are comparatively large and well spaced (the M_6C in Fig. 9) the nucleation of new recrystallized grains will be accelerated, but if they are small and closely spaced (the Mo_2C in Fig. 9) nucleation will be retarded or prevented altogether. Subsequently, however, the M_6C particles will impede the growth of the new grains, and there is ample evidence for this in Fig. 9.

The discontinuous reaction product of Fig. 10 is probably a result of retained austenite decomposition at 700° C. Cohen [16] has shown that the mechanism by which retained austenite decomposes depends on the stability of the austenite. In plain carbon and low alloy steels where the retained austenite is not very stable, decomposition

Figure 10 Discontinuous precipitation in splat-cooled Fe–10% Mo–0.5% C aged 1 h at 700° C. Ion-beam thinned foil. Transmission electron micrograph.

to bainite occurs during heating above 120° C. This was observed in the splat-cooled Fe–4% Mo–0.2% C alloy, for which differential thermal analysis indicated the disappearance of austenite in the range 220 to 400° C. On the other hand, in high-speed and other highly alloyed steels, retained austenite does not decompose isothermally to any considerable extent during normal tempering in the range 550 to 600° C; instead, "conditioning" causes changes in the austenite (such as carbide precipitation and relaxation of stresses [33]) that render it unstable on cooling, and it transforms to martensite. However, if tempering is carried out above the normal temperature range, retained austenite can isothermally transform to pearlite in highly alloyed steels [34].

It is proposed that a similar reaction occurs in the splat-cooled Fe–10% Mo–0.5% C alloy, except that the pearlite in this case is an alloy pearlite, with the carbide lamellae having the composition Mo_2C. Support for this contention comes from the results described earlier in which retained austenite gave no decomposition peak on heating in the differential thermal analyser to 600° C, but was found to disappear on isothermal holding between 1 h at 550° C and 1 h at 600° C. Furthermore, the fact that the alloy pearlite was observed rarely, is in agreement with the X-ray analysis which showed that the splat-cooled alloy contained only 0 to 10% retained austenite.

5. Conclusions

(1) In an Fe–4% Mo–0.2% C alloy, splat cooling produces a phase mixture of δ-ferrite, martensite, and austenite, the amount of austenite increasing with decreasing cooling rate. There is no segregation evident in the microstructure of any phase, except for the presence of rows of dislocation loops in the austenite.

(2) Splat cooling of an Fe–10% Mo–0.5% C alloy produces a phase mixture of δ-ferrite, martensite, austenite and Mo_2C, the δ-ferrite being the most abundant phase. Solute segregation during solidification induces the formation of carbide particles at the dendrite boundaries of the δ-ferrite. The extent of interdendritic carbide formation is greater the larger the splat thickness and in thicker areas precipitation of Mo_2C needles within the δ-ferrite dendrites also occurs. Lattice parameter measurements indicate that a higher supersaturation is achieved in the δ-ferrite of the splat-cooled alloy than in the martensite of water-quenched filings.

(3) In both splat-cooled alloys finely-twinned martensite is formed which is different from the dislocated lath martensite found in the corresponding water-quenched alloys. The morphology change is caused by a combination of the greater cooling rate and smaller section thickness of the former.

(4) The absence of solute segregation in the Fe–4% Mo–0.2% C alloy and its presence in the Fe–10% Mo–0.5% C alloy is a reflection of the degree of undercooling achieved relative to the equilibrium liquidus–solidus temperature range of the respective alloys.

(5) Upon ageing, Mo_2C precipitates in the ferrite matrix of both alloys in the usual orientation relationship. In the more concentrated alloy precipitation of M_6C and recrystallization of ferrite occur in areas of local inhomogeneity. Retained austenite in this alloy decomposes isothermally between 550 and 600° C to an alloy pearlite, whereas in the Fe–4% Mo–0.2% C alloy the austenite decomposes to bainite during heating in the range 220 to 400° C.

Ackowledgements

One of us (IRS) is grateful for the award of a CSIRO postgraduate Studentship.

References

1. D. RAYNOR, J. A. WHITEMAN and R. W. K. HONEYCOMBE, *J. Iron Steel Inst.* **204** (1966) 349.
2. *Idem, ibid.* **204** (1966) 1114.
3. R. C. RUHL and M. COHEN, *Trans. Met. Soc. AIME* **245** (1969) 241.
4. M. HANSEN and K. ANDERKO, "Constitution of Binary Alloys", 2nd edn (McGaw–Hill, New York, 1958).
5. R. C. RUHL and M. COHEN, *Trans. Met. Soc, AIME* **245** (1969) 253.
6. A BROWN, Ph.D. Dissertation, University of Cambridge (1973).
7. J. ZBORIL and Z. POSEDEL, *Z. Metallk.* **61** (1970) 214.
8. J. V. WOOD and I. R. SARE, Proceedings of the Second International Conference on Rapidly Quenched Alloys, edited by N. J. Grant and B. C. Giessen (MIT Press, Cambridge, Mass., 1976) p. 87.
9. C. S. ROBERTS, B. L. AVERBACH and M. COHEN, *Trans. ASM* **45** (1953) 576.
10. P. RAMACHANDRARAO, P. RAMA RAO and T. R. ANANTHARAMAN, *Z. Metallk.* **61** (1970) 471.
11. A. KIRIN and A. BONEFACIC, *J. Phys. F: Metal Phys.* **4** (1974) 1608.
12. J. WOOD and I. SARE, *Met Trans. A.* **6A** (1975) 2153.
13. J. V. WOOD and R. W. K. HONEYCOMBE, *J. Mater. Sci.* **9** (1974) 1183.
14. W. PITSCH and A. SCHRADER, *Arch. Eisenhüttenw.* **29** (1958) 715.
15. G. R. SPEICH, *Trans. Met. Soc, AIME* **224** (1962) 850.
16. M. COHEN, *Trans. ASM* **41** (1949) 35.
17. H. R. WOEHRLE, W. R. CLOUGH and G. S. ANSELL, *ibid.* **59** (1966) 784.
18. R. W. MESSLER, G. S. ANSELL and V. I. LIZUNOV, *ibid.* **62** (1969) 362.
19. Y. INOKUTI and B. CANTOR, *Scripta Met.* **10** (1976) 655.
20. W. T. OLSEN and R. HULTGREN, *Trans. AIME* **188** (1950) 1323.
21. H. BILONI and B. CHALMERS, *Trans. Met. Soc. AIME* **233** (1965) 373.
22. K. LÖHBERG and H. MÜLLER, *Z. Metallk.* **60** (1969) 231.
23. "Metals Handbook", 8th edn, Vol. 8 (ASM, Ohio, 1973) p. 410.
24. I. S. MIROSHNICHENKO and G. P. BREKHARYA, *Phys. Met. Metallog.* **29** (1970) 233.
25. G. S. ANSELL, S. J. DONACHIE and R. W. MESSLER, *Met. Trans.* **2** (1971) 2443.
26. S. J. DONACHIE and G. S. ANSELL, *Met Trans. A.* **6A** (1975) 1863.
27. W. PITSCH, *Phil. Mag.* **4** (1959) 577
28. *Idem, J. Inst. Metals* **87** (1959) 444.
29. H. WARLIMONT, *Trans. Met. Soc. AIME* **221** (1961) 1270.
30. J. GAGGERO and D. HULL, *Acta Met.* **10** (1962) 995.
31. K. KUO, *J. Iron Steel Inst.* **173** (1953) 363.
32. R. W. CAHN " Physical Metallurgy", 2nd revised edn, edited by R. W. Cahn (North-Holland, London, 1970) p. 1129.
33. E. C. ROLLASON, "Fundamental Aspects of Molybdenum on Transformation of Steel" (Climax Molybdenum, London, 1962).
34. R. W. BALLUFFI, M. COHEN and B. L. AVERBACH, *Trans. ASM* **43** (1951) 497.

Received 20 December 1977 and accepted 19 January 1978.